FULL PAPER DOI: 10.1002/adsc.201900134 Advanced Synthesis & Catalysis

Structure-Guided Evolution of Aryl Alcohol Oxidase from *Pleurotus eryngii* for the Selective Oxidation of Secondary Benzyl Alcohols

Javier Viña-Gonzalez,[a] Diego Jimenez-Lalana,[a] Ferran Sancho,[b] Ana Serrano,[c] Angel T. Martinez,[c] Victor Guallar,[b, d] and Miguel Alcalde[a,*]

[a] Department of Biocatalysis, Institute of Catalysis, CSIC, Cantoblanco, 28049 Madrid, Spain
Fax: (+31)-91 5854760; phone: (+34)-91 5854806
E-mail: malcalde@icp.csic.es
[b] Barcelona Supercomputing Center, Jordi Girona 31, 08034 Barcelona, Spain
[c] Biological Research Center, CSIC, Ramiro de Maeztu 9, 28040 Madrid, Spain
[d] ICREA, Passeig Lluís Companys 23, 08010 Barcelona, Spain

Manuscript received: January 29, 2019; Revised manuscript received: March 7, 2019;
Version of record online: April 4, 2019

Supporting information for this article is available on the WWW under https://doi.org/10.1002/adsc.201900134

Abstract: Aryl alcohol oxidase (AAO) is a fungal flavoenzyme capable of oxidizing aromatic primary alcohols into their correspondent aldehydes through a stereoselective hydride abstraction. Unfortunately, this enzyme does not act on secondary benzyl alcohols in racemic mixtures due to the strict control of substrate diffusion and positioning at the active site restricted to primary benzyl alcohols. Here we describe the engineering of AAO from *Pleurotus eryngii* to oxidize chiral benzyl alcohols with high enantioselectivity. The secondary benzyl alcohol oxidase was remodeled at the active site through four cycles of structure-guided evolution, including a final step of *in vivo* site-directed recombination to address the positive epistatic interactions between mutations. The final variant, with five substitutions and a renovated active site, was characterized at biochemical and computational level. The mutational sculpting helped position the bulkier (S)-1-(*p*-methoxyphenyl)-ethanol, improving the mutant's catalytic efficiency by three orders of magnitude relative to the native enzyme while showing a high enantioselectivity (ee >99%). As a promising candidate for racemic resolution, this evolved secondary benzyl alcohol oxidase maintained its natural stereoselective mechanism while displaying activity on several secondary benzyl alcohols.

Keywords: aryl alcohol oxidase; secondary benzyl alcohols; *Saccharomyces cerevisiae*; directed evolution

Introduction

With global annual sales of $ 1 trillion, an increasingly important challenge in drug development that the pharmaceutical sector must overcome is that posed by chiral chemistry.[1] Indeed, enantiopure building blocks are in strong demand to produce drugs with particular biological activities, while they are also paramount for the production of fine chemicals.[2] Biocatalysis has found an important niche in the field of chiral technology, with enzymatic and whole-cell biotransformations offering stereo-, regio- and chemio-selectivity under mild reaction conditions. Classically, two fundamental approaches are followed in the industrial production of chiral molecules: enantioselective synthesis and racemic mixture separation. While asymmetrical synthesis involves complex and expensive processes,[3] dynamic kinetic resolution (DKR) is currently one of the most efficient sources of chiral molecules, in which separation is coupled to the in situ re-racemization of one of the enantiomers. Another recently described transformative source of enantiomers is cyclic de-racemization. Based on cyclic oxidation-reduction sequences, after the selective oxidation of one of the enantiomers, the achiral intermediate (ketone or imine) is non-selectively reduced to the racemic initial material. After a certain number of cycles, a theoretical 100% yield of the non-reactive enantiomer can be accumulated.[4] The core step in racemic separation, kinetic resolution, has been achieved for secondary alcohols using either whole-cell systems[5] or isolated enzymes, such as alcohol

dehydrogenases,[6] lipases[7] and particularly, oxidases.[8] This latter solution is the simplest means to prepare optically pure secondary benzyl alcohols, given their trivial requirements (only needing O_2 from the air) and high enantioselectivity.[8a,9]

Among these enzymes, aryl alcohol oxidase (AAO, EC 1.1.3.7) is a promising candidate for the enantioselective oxidation of chiral benzyl alcohols. AAO is a flavoenzyme belonging to the GMC (glucose-methanol-choline) superfamily of oxidoreductases and it is naturally secreted as a part of the fungal enzymatic consortium involved in lignin degradation.[10] Accepting a variety of aromatic alcohols as substrates, the activity of AAO is initially divided into two half-reactions. The first reductive half-reaction involves highly enantioselective hydride transfer from the alcohol's α-C to the FAD co-factor. This process yields the corresponding aldehyde, such that the FAD can then be reoxidized by O_2, releasing H_2O_2 as a by-product of the second oxidative half of the reaction.[11] Unfortunately, the active site of AAO is buried under a hydrophobic constriction formed by residues Tyr92, Phe397 and Phe501. As a result, substrates bulkier than primary aromatic alcohols cannot easily be accommodated, reducing the enzyme's activity on chiral molecules to a residual trace. Until recently the failure to functionally express AAO in an appropiate heterologous host had prevented its directed evolution. However, fusing the enzyme to a chimeric signal prepro-leader has enabled this protein to be successfully evolved for secretion by yeast.[12]

Taking advantage of this expression system, here we have combined different laboratory evolution strategies to unlock the activity of AAO on secondary aromatic alcohols. We first carried out a carefully structure-guided campaign of evolution using chiral 1-(*p*-methoxyphenyl)-ethanol as the substrate, thereby generating a palette of secondary benzyl alcohol oxidase mutants. Employing *in vivo* site-directed recombination approaches, mutations were curated by comparing them with their correspondent parental reversions. The differential oxidation of secondary benzyl alcohols by the final benzyl alcohol oxidase variant was characterized, while the rationale behind these changes was analyzed computationally at the atomic level.

Results and Discussion

Laboratory Evolution

First Generation: Unlocking Activity for Secondary Aromatic Alcohols

The departure point of this study was a secretion mutant of the AAO from *Pleurotus eryngii* named FX9. This mutant is the product of several rounds of directed evolution aimed to promote functional expression in *Saccharomyces cerevisiae*.[12] In this FX9 variant, the AAO is fused to a chimeric prepro-leader (preα-factor-proKiller) that enhanced secretion by introducing the F[3α]S, N[25proK]D, T[50proK]A and F[52proK]L mutations into the pre-α and pro-Killer leaders. In addition, two substitutions were included in the mature AAO: L170M in an α-helix situated at the protein surface, and the consensus, ancestral mutation H91N in the FAD attachment loop. These latter mutations enhanced stability and improved production by *S. cerevisiae* to 4.5 mg/L and by *Pichia pastoris* in bioreactor to 25.5 mg/L, while conserving the general biochemical features of the native AAO.[12]

As a substrate for the screening assay we chose 1-(*p*-methoxyphenyl)-ethanol, a chiral molecule with similar structure to the natural *p*-methoxybenzyl alcohol substrate, the oxidation of which by AAO can be rapidly assessed in a coupled Amplex Red/HRP assay (see Experimental Section for details). As the activity of AAO on secondary alcohols is irrelevant, no response was detected with 1-(*p*-methoxyphenyl)-ethanol when the parental FX9 was screened in microtiter fermentations of the supernatant (i.e. cultures in 96 well plates). As indicated previously, AAO's failure to oxidize secondary aromatic alcohols is due to steric perturbation of the residues forming the catalytic cavity when trying to accommodate bulkier, chiral molecules. Specifically, Phe501 is thought to be a steric liability at the active site, particularly given the very weak but detectable activity on 1-(*p*-methoxyphenyl)-ethanol of a F501A variant expressed in *E. coli* after *in vitro* refolding.[21] A more recent rational attempt to achieve secondary alcohol oxidation based on PELE (Protein Energy Landscape Exploration) suggested Ile500 was another possible obstacle for ligand diffusion. Indeed, the I500A substitution conferred better transit of the substrate to the active site due to channel broadening.[22]

To ensure that the activity on secondary benzyl alcohol could be measured at the start of the laboratory evolution campaign, we first prepared three mutants from the FX9 secretion variant: I500A, F501A and I500A-F501A (Figure S2A, B). When isolated from yeast supernatants these variants did not appear to act on 1-(*p*-methoxyphenyl)-ethanol. Hence, we performed combinatorial saturation mutagenesis of the Ile500-Phe501 residues and we found several clones with activity on 1-(*p*-methoxyphenyl)-ethanol, which were scaled up to a 100 mL flask to estimate the overall improvement in activity. Of these, the I500Q-F501W, I500L-F501I, I500M-F501V and I500M-F501W mutants presented a 5-, 15-, 30- and 160-fold enhancement in activity relative to the parental FX9, respectively. The activity of the I500M-F501W mutant (named 15G12) was further tested against a panel of primary and secondary alcohols (Table 1). Its specific activity on primary alcohols was dramatically reduced

Table 1. Specific activity of AAO variants with primary and secondary alcohols.

	Benzyl alcohol	Cinnamyl alcohol	*p*-Methoxy benzyl alcohol	*p*-Chloro benzyl alcohol	3,4-Dimethoxy benzyl alcohol	2,4-Hexadien-1-ol	1-Phenyl ethanol	*p*-Fluoro-α-methyl benzyl alcohol	1-(*p*-Methoxyphenyl)-ethanol
	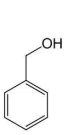	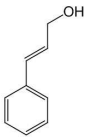	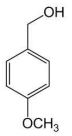	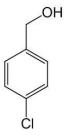	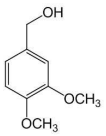	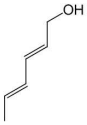	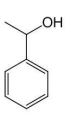	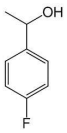	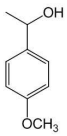
FX9 (U/mg)	15.6	41.1	46.6	26.6	22.2	43.4	n.d.	n.d.	$2.2x10^{-3}$
15G12 (U/mg)	0.6	18.4	0.3	0.6	0.03	13	$6x10^{-3}$	$6x10^{-3}$	0.3

Specific activities were estimated in 100 mM phosphate buffer pH 6.0 containing 5 mM of each alcohol. Each reaction was performed by triplicate and substrate conversion was followed by measuring the absorption at 563 nm ($\varepsilon_{563} = 56000\ M^{-1}\,cm^{-1}$) using the HRP/Amplex red coupled assay as described in the experimental section.

depending on the chemical nature of the molecule, with practically no activity on *p*-methoxybenzyl alcohol (c.a. 0.6% of that of the parental FX9 variant). By contrast, the activity of the 15G12 variant on secondary aromatic alcohols rose from undetectable levels, to weak yet evident activity on 1-phenylethanol and 4-fluoro-α-methylbenzyl alcohol, and up to 0.3 U/mg on 1-(*p*-methoxyphenyl)-ethanol (Table 1). Given that hydride abstraction of *p*-methoxybenzyl alcohol to the flavin of AAO occurs exclusively from the pro-R position, in deracemization reactions of secondary alcohols hydrogen abstraction should produce S enantioselective oxidation of the alcohol to the corresponding ketone.

To confirm this, reactions were performed with the optically pure (R) and (S)-4-fluoro-α-methylbenzyl alcohol enantiomers, and as expected, only activity on the latter was detected.[23]

Paradoxically, while the initial search for a wider space for secondary aromatic alcohol accommodation focused on the I500A-F501A mutations, the bulky alcohol would appear to be much better oxidized in a narrower catalytic pocket following the substitution of Ile500 and Phe501 by the more expansive Met and Trp, respectively (Figure S2C, D). Thus, these two mutations at the active site reposition the secondary alcohol, favouring catalysis, as confirmed by computational analysis (see below).

Second and Third Generations: Searching for new Beneficial Mutations

After unlocking the activity on secondary benzyl alcohols, different protein segments of the 15G12 mutant were targeted for random mutagenesis and DNA recombination by MORPHING, with a view to further optimize its activity on secondary alcohols. This focused structural evolution tool allows the protein to be divided into defined mutagenic areas, each of which can be interrogated in conjunction with the *in vivo* recombination of the different DNA fragments in *S. cerevisiae*.[14] This approach has already been successfully applied during the evolution of AAO towards functional expression in yeast[12] and on this occasion, the design involved the study of three protein blocks in independent libraries (Figure 1A, B). The first of these was the MA block at the N-terminus (Leu48-Thr100), which is associated with the access channel and the FAD-binding domain, and that contains important determinants like Pro79, Asn91, Tyr92 and Val90.

The second MB block (Leu310-Ile417) covers the wall of the catalytic pocket and it contains the aromatic Phe397, a residue implicated in substrate positioning and product release. The third MC block (Glu490-Gln566) is situated in the C-terminal region, and it contains the catalytic His502 and several amino acids related to substrate positioning (Met500, Trp501 and His546). Together, these three blocks encompass the complete active site and the aromatic bottleneck formed by Tyr92, Phe397 and Trp501 (Figure 1C).[16,23,24]

We carried out the three independent libraries of MORPHING; besides, we prepared a conventional error-prone PCR (ep-PCR) mutagenic library that targeted the whole AAO gene (in total over 4,000 clones were screened). From the pool of libraries, seven mutants with stronger activity on the secondary 1-(*p*-methoxyphenyl)-ethanol were selected for further analysis, ranging from a 1.4 to 2.2-fold enhancement

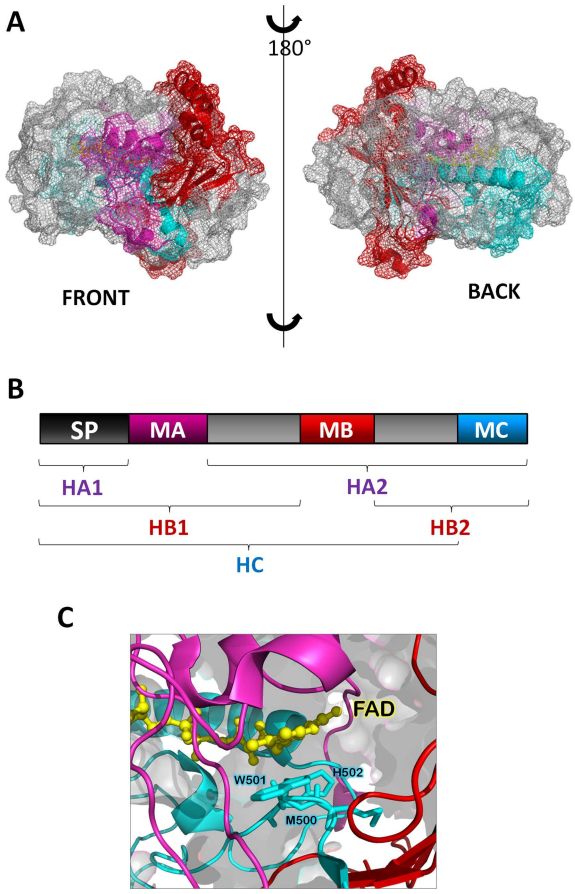

Figure 1. MORPHING fragments for focused evolution. (A) Front and back views of AAO, with the MA, MB and MC MORPHING blocks shown in purple, red and blue, respectively. (B) The dark grey box corresponds to the signal peptide, and the three mutagenic fragments considered for MORPHING are shown as purple, red and blue boxes. For the first MORPHING library, mutagenic block MA was *in vivo* assembled with high-fidelity fragments HA1 and HA2. For the second library, mutagenic fragment MB was recombined from high-fidelity fragments HB1 and HB2. The third library was constructed with the assembly of mutagenic block MC and high-fidelity fragment HC. (C) The catalytic pocket of AAO with the contribution of the MORPHING blocks MA, MB and MC (purple, red and blue, respectively). Model prepared with the crystal structure of the AAO from *P. eryngii* (PDB 3FIM).

over 15G12 (Figure 2). The most successful MORPHING corresponded to the MA block, with five of the seven improved AAO variants from this library. Interestingly, all the mutations identified were located within a 14 amino acid span, from Ile76 to Val90. The mutations carried by the best variant (3F10) were I76V and M83I, which in conjunction with the rest of the substitutions in this stretch (A77V, R80C, I76V and V90A) highlight the importance of the access channel in modulating oxidative activity. Indeed, it should be noted that the R80C substitution was also found in the triple 6G3 mutant from the whole gene ep-PCR library, together with two superficial substitutions: E39G and Q466R (Figure 2). The MORPHING method was also successful in fragment MB, where the 12D12 variant presented two mutations at the surface: F332L and V340A. Applying focused mutagenesis to the area corresponding to the catalytic pocket, the MC block, was ineffective since variants with improvements were not detected.

To further enhance secondary alcohol oxidation, the best variants from each library were submitted to ep-PCR and *in vivo* shuffling in *S. cerevisiae*: 3F10 and 11H2 from the MA library, the 12D2 variant from the MB library, and the 6G3 variant obtained through whole-gene mutagenic amplification. From this third generation, the 3C11 variant was seen to enhance the activity roughly 1.2-fold compared to 3F10 (412-fold relative to the FX9 parental type), retaining the I76V mutation from 3F10 and acquiring the V90A change, also previously detected in the 9F2 variant, as well as incorporating the new Q174R substitution (Figure 2).

Fourth Generation: Mutational Polishing by in vivo site-directed Recombination

After careful evaluation of the mutations obtained in the second and third generations (Table 2), we decided to undertake a final round of evolution to assess whether there were any positive epistatic effects among the mutations. We constructed a combinatorial library by *in vivo* site-directed recombination, such that the 10 mutations and their corresponding reversions could be rapidly combined in an one-pot transformation reaction, evaluating the library in order to obtain the optimal combination of substitutions for the oxidation of chiral alcohols (Figure S1). From this ensemble of mutations, the three best variants identified shared the same backbone of substitutions: A77V-R80C-V340A. The third best variant was the 24H3 mutant that carried the A77V-R80C-Q174R-F332L-V340A-Q466R muta-

Table 2. Selected mutations for site-directed recombination.

Mutation	Variant	Library	Secondary motif
$_{GAG}$E39G$_{GGG}$	6G3	ep-PCR	Loop
$_{ATT}$I76V$_{GTT}$	3F10, 4D8	MA	Loop
$_{GCG}$A77V$_{GTG}$	11H2	MA	Loop
$_{CGC}$R80C$_{TGC}$	6G3, 7B4	ep-PCR, MA	Loop
$_{ATG}$M83I$_{ATA}$	3F10	MA	Loop
$_{GTT}$V90A$_{GCT}$	9F2	MA, mutagenic shuffling	Loop
$_{CAA}$Q174R$_{CGA}$	3C11	Mutagenic Shuffling	Alpha helix
$_{TTC}$F332L$_{CTC}$	12D2	MB	Alpha helix
$_{GTT}$V340A$_{GCT}$	12D2	MB	Alpha helix
$_{CAA}$Q466R$_{CGA}$	6G3	ep-PCR	Loop

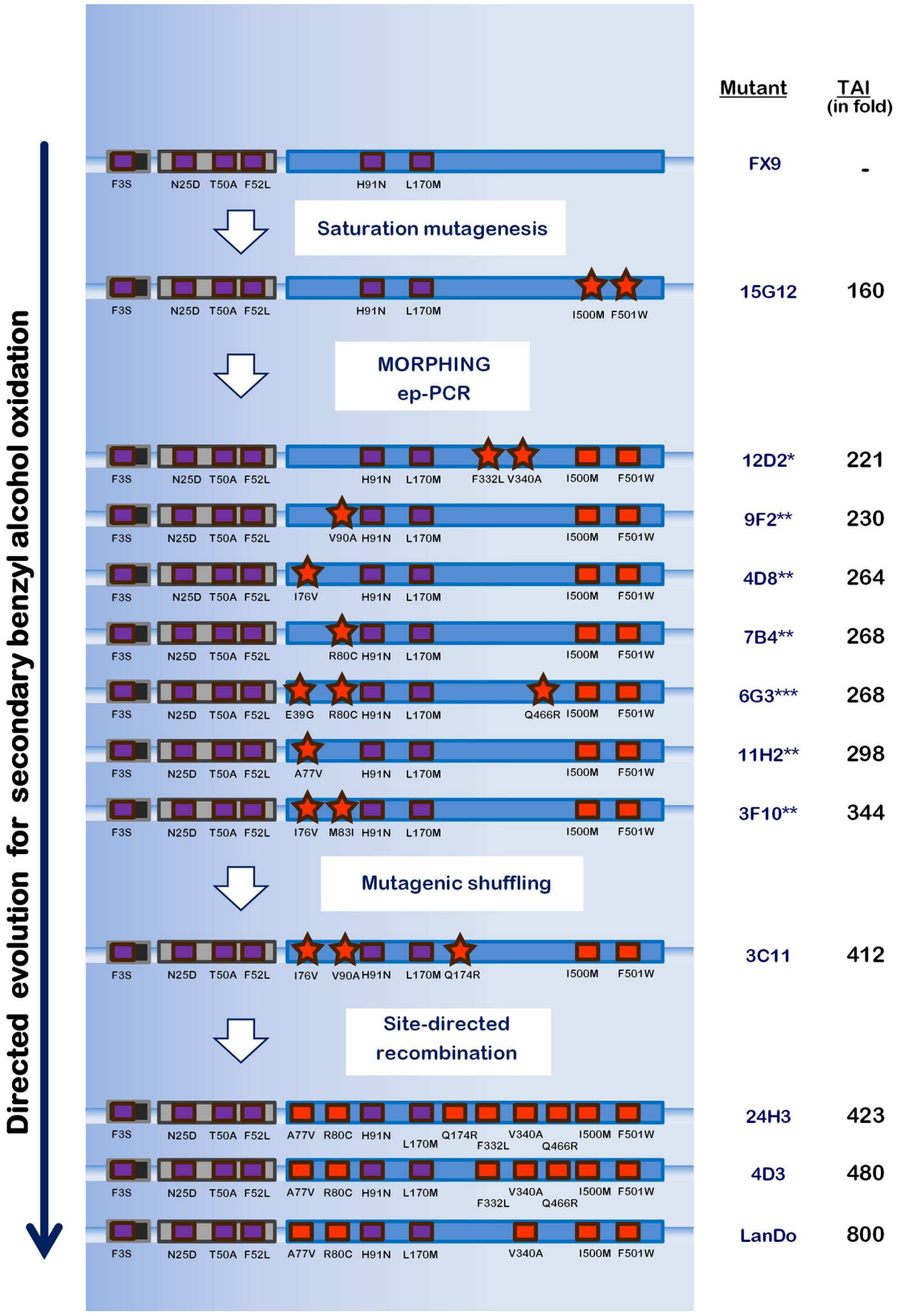

Figure 2. Laboratory evolution of AAO for the oxidation of secondary benzyl alcohols. New mutations are represented as stars and accumulated mutations as squares. The chimeric prepro-leader is depicted in grey and the mature AAO in blue. The TAI (total activity improvement) refers to the fold improvement of AAO activity with 1-(*p*-methoxyphenyl)-ethanol as a substrate and it was estimated relative to the FX9 parental type from *S. cerevisiae* supernatants: *Mutants from the MB library; **Mutants from the MA library; ***Mutant from the ep-PCR library.

tions, displaying activity more than 420-fold better than the FX9 parental type. In the case of 4D3, the only difference from the 24H3 variant was the absence of the Q174R mutation, which translated into a 480-fold increase in activity, highlighting a detrimental effect of Q174R within this mutational context. The further purging of Q466R and F332L gave rise to the LanDo variant that carried the A77V-R80C-V340A mutations in conjunction with I500M-F501W and the 6 secretion mutations of FX9, this variant representing the best performer with a total 800-fold enhancement of activity relative to the parental type (Figures 2, 3).

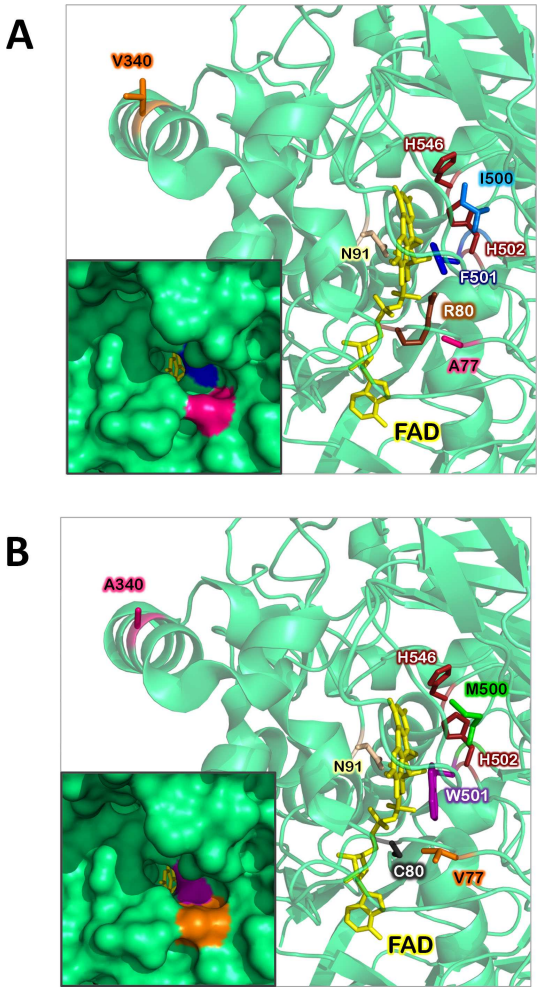

Figure 3. Location of the mutations in the evolved secondary benzyl alcohol oxidase. (A) FX9 parental type and (B) LanDo mutant. The FAD molecule is represented in yellow, the catalytic base His502 and His546 is depicted in red, and the consensus ancestral mutation Asn91 is in light pink. A77V, R80C, V340A, I500M and F501W are represented following a color code (before and after mutation). The mutation L170M at the surface of the enzyme is not present in the fragment represented. The inset shows a detail of the protein surface at the access channel. The model was prepared with a crystal structure of the AAO from *P. eryngii* (PDB 3FIM).

Biochemical Characterization

To characterize the LanDo mutant and the FX9 parental variant, they were produced and purified to homogeneity. To determine the enantioselectivity of the LanDo variant, transformation of the racemic 1-(*p*-methoxyphenyl)-ethanol was followed by chiral-HPLC (Figure 4) and 100% conversion with an enantiomeric

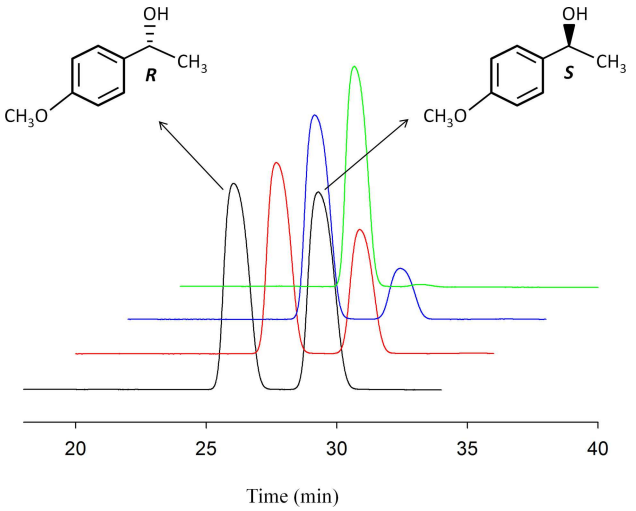

Figure 4. Chiral HPLC analysis. HPLC elution profiles after the reaction of the AAO variant LanDo (1 μM) with racemic 1-(*p*-methoxyphenyl)-ethanol (2.5 mM). Reactions were performed at room temperature in 100 mM phosphate buffer pH 6.0 with continuous shaking and the aliquots were analyzed by chiral HPLC at different times. The separation of the R and S enantiomers in the negative control is represented in black, whereas the 15, 45, and 90 min reactions are represented in red, blue and green, respectively.

excess (ee) >99% was achieved after a two hour reaction. The configuration of the remaining alcohol in the reaction was confirmed by optical rotation (Figure S3, Table S2), the positive rotation corresponding to the R enantiomer meaning the natural oxidation of the S enantiomer by AAO was maintained after evolution.[23] Despite the remarkably specific activity for the secondary 1-(*p*-methoxyphenyl)-ethanol (2.9 U/mg), the five new mutations carried by the LanDo variant did not negatively affect its secretion (4.6 mg/L). The activity of LanDo with secondary alcohols was tested against available commercial secondary (aromatic) alcohols that were representative of the structural scope of the AAO. The initial turnover rates of the LanDo variant relative to the wildtype AAO (wtAAO, heterologous expressed in *E. Coli* after *in vitro* refolding) increased 30, 20 and 100-fold times for 1-(*p*-methoxyphenyl)-ethanol, *p*-fluoro-α-methyl-benzyl alcohol and 1-phenylethanol, respectively. Indeed, the LanDo variant even showed activity on 1-

phenylpropanol, a substrate not oxidized by wtAAO (Table 3). The kinetic parameters were measured under

Table 3. Initial turnover rates for secondary alcohols.

	p-Fluoro-α-methyl-benzyl alcohol	1-Phenyletha-nol	1-Phenylpropa-nol
wtAAO	0.35 ± 0.01	0.10 ± 0.03	n.m.
LanDo	7.3 ± 0.1	10 ± 0.5	1 ± 0.1

Turnover rates (min^{-1}) were estimated in 100 mM phosphate buffer pH 6.0 containing 5 mM of each secondary alcohol with the exception of 1-phenylpropranol (2.5 mM). Each reaction was performed by triplicate and substrate conversion was followed by measuring the absorption at 563 nm ($\varepsilon_{563} = 56000\ M^{-1}\,cm^{-1}$) using the HRP/Amplex red coupled assay as described in the experimental section.

air-saturated conditions for 1-(*p*-methoxyphenyl)-ethanol, and for the primary alcohols *p*-methoxybenzyl alcohol and 2,4-hexadien-1-ol. LanDo displayed an outstanding increase in the catalytic efficiency for enantioselective oxidation of 1-(*p*-methoxyphenyl)-ethanol, three orders of magnitude. Interestingly, the activity on primary alcohols that was dramatically reduced after inserting the I500M-F501 W pair in the first cycle of evolution in 15G12 variant (Table 1, Figure 2), was recovered to a considerable extent for *p*-methoxybenzyl alcohol and the aliphatic 2,4-hexadien-1-ol. This result indicates the beneficial effect that A77V, R80C and V340A exerted on LanDo's overall activity (Table 4).

Computational Analysis

In order to rationalize the effect of the mutations identified, PELE simulations were run for wtAAO and the variants obtained in the different rounds of directed evolution. The oxidation of alcohols by AAO involves a non-synchronous concerted reaction, where both proton transfer from the hydroxyl group to the catalytic base His502 and hydride abstraction from the benzylic position by the flavin are taking place at the same reaction step.[11] PELE results were plotted placing both catalytic distances in the X and Y axis, and the interaction energy between the protein and the ligand was represented by colors (Figure 5).

No significant differences were evident between the wtAAO and the secretion mutant FX9 (H91N-L170M) in these plots, consistent with the experimental evidence that this variant does not improve the activity on secondary alcohols but does increase expression and stability. The 15G12 variant included the I500M and F501W mutations on top of the previous ones, accumulating a total of 4 mutations in the mature protein. In this case, the plot shows how the ligand can reach catalytic positions 2.5 Å away from both the FAD and the histidine at the same time, producing better catalytic constants than those of the wtAAO. In addition, a minimum could be seen where the ligand-histidine distance was ~2.2 Å, although the interaction energies were much higher and they were therefore less accessible.

The largest improvement came after introducing an additional three mutations in the LanDo variant: A77V, R80C, and V340A. These three substitutions allow the ligand to achieve even smaller catalytic distances, up to ~2 Å for the histidine and 2.4 Å for the FAD, with reasonable interaction energies. Considering that closer catalytic distances imply a decrease in energy barriers, this agreed well with the higher kinetic constants. Moreover, the increase in the number of structures with good catalytic distances could reflect the ease with which the ligand can find catalytic positions, explaining the lower K_m values for this variant.

Despite the large number of mutations in LanDo (7 in total, excluding the mutations in the chimeric prepro-leader), there are no major conformational changes in the protein or in the positioning of the ligand. Nevertheless, we did note subtle modifications that were sufficient to improve the catalytic position of

Table 4. Kinetic parameters for AAO variants.

Substrate	Kinetic constants	wtAAO**	LanDo
1-(*p*-methoxyphenyl)-ethanol	K_m (mM)*	24.9 ± 1.1	0.65 ± 0.1
	k_{cat} (s^{-1})	0.18 ± 0.002	4.9 ± 0.1
	k_{cat}/K_m ($mM^{-1}\,s^{-1}$)	0.007	7.5
p-methoxybenzyl alcohol**	K_m (mM)	0.027 ± 0.004	0.02 ± 0.003
	k_{cat} (s^{-1})	142 ± 5	72 ± 3
	k_{cat}/K_m ($mM^{-1}\,s^{-1}$)	5233	3600
2,4-hexadien-1-ol**	K_m (mM)	0.094 ± 0.005	0.095 ± 0.006
	k_{cat} (s^{-1})	119 ± 2	40.9 ± 0.7
	k_{cat}/K_m ($mM^{-1}\,s^{-1}$)	1271	430.5

AAO kinetic constants were measured in 100 mM phosphate buffer pH 6.0 at 25 °C. All reactions were performed by triplicate. *Referred to the S enantiomer, as 50% of the racemic mixture. **Calculated for wtAAO as described previously.[22,26]

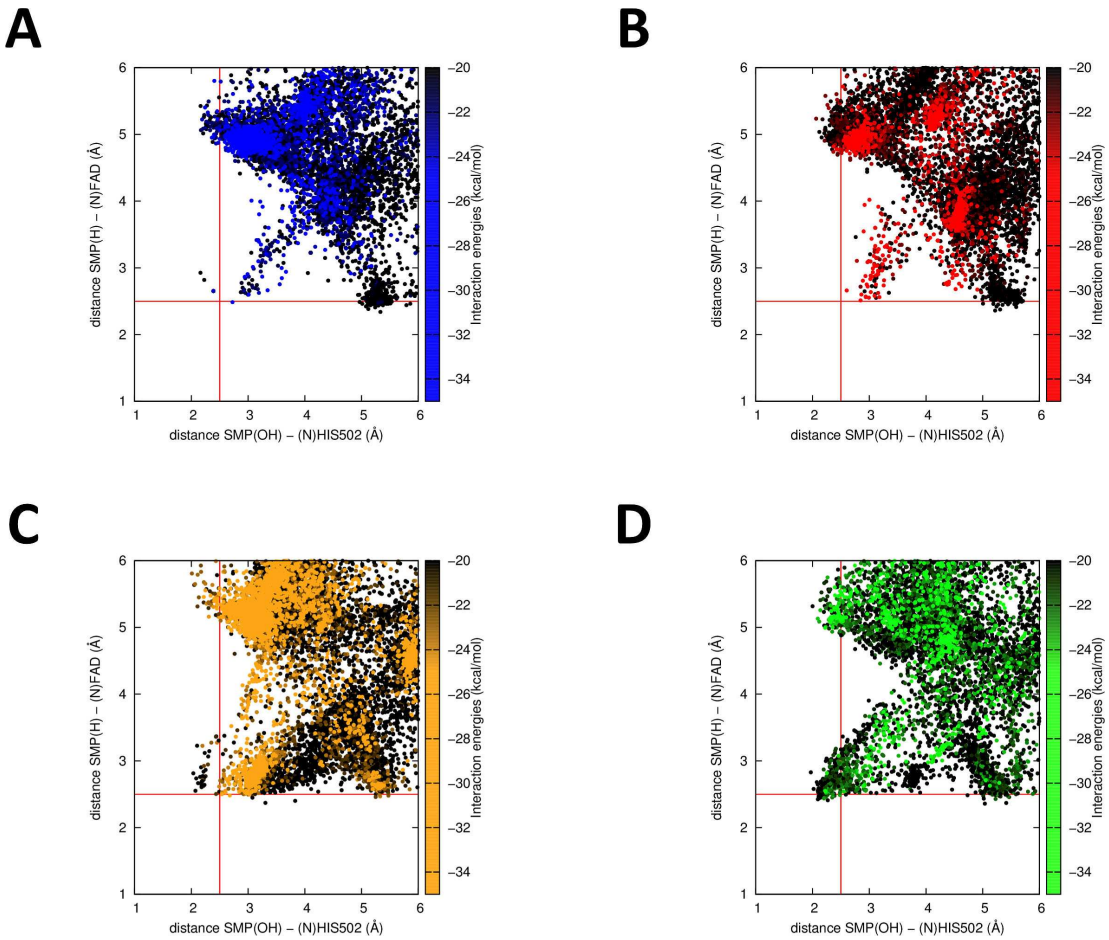

Figure 5. Substrate diffusion computational PELE simulations. Plots represent the PELE simulations relating catalytic distances (X and Y) and interaction energies (color scheme, right Y axis) for different AAO variants: (A) wtAAO; (B) the FX9 secretion mutant; (C) the 15G12 mutant; (D) the final evolved benzyl alcohol oxidase, LanDo mutant.

(S)-1-(*p*-methoxyphenyl)-ethanol. In particular, the R80C mutation was found repeatedly in independent libraries during evolution (Figure 2) and it created an empty space at the top of the FAD cofactor. Consequently, the backbone containing H502 shifts in that direction (Figure 6A). Moreover, Arg80 interacts with the oxygen of the backbone of residue 501, such that this mutation frees Trp501 to form a hydrogen bond with the oxygen backbone of Val77 (Figure 6B). All these subtle adjustments allow the ligand to adopt conformations with better catalytic distances (Figures 5, 6).

Conclusion

Focusing evolution on structural elements made it possible to identify mutations in the catalytic pocket and access channel that allowed an AAO to be designed that acts on different secondary benzyl alcohols. This final secondary benzyl alcohol oxidase variant maintained strong enantioselectivity, providing a potential catalyst for chiral de-racemization. The complex enzyme-substrate relationships of this enzyme were highlighted by an enhancement of three orders of magnitude in the catalytic efficiency, an effect produced by a combination of bulky substitutions in the catalytic cavity and other unpredicted changes. Paradoxically, a steric problem appeared to be resolved by introducing bulkier residues, something difficult to anticipate from a rational point of view. It is worth noting that the resolution of molecules like 1-phenylpropanol could be of use to obtain moiety precursors of serotonin/norepinephrine reuptake inhibitors like Fluoxetine or Atmoxetine.[6]

The results obtained here also highlight the importance and efficacy of *S. cerevisiae* as a platform for both the functional expression of eukaryotic genes and as a molecular tool-box to generate DNA libraries for directed evolution campaigns. The data presented open new opportunities for the evolution of AAO, which include the oxidation of furfural derivatives for the synthesis of biopolymers or the *in situ* production

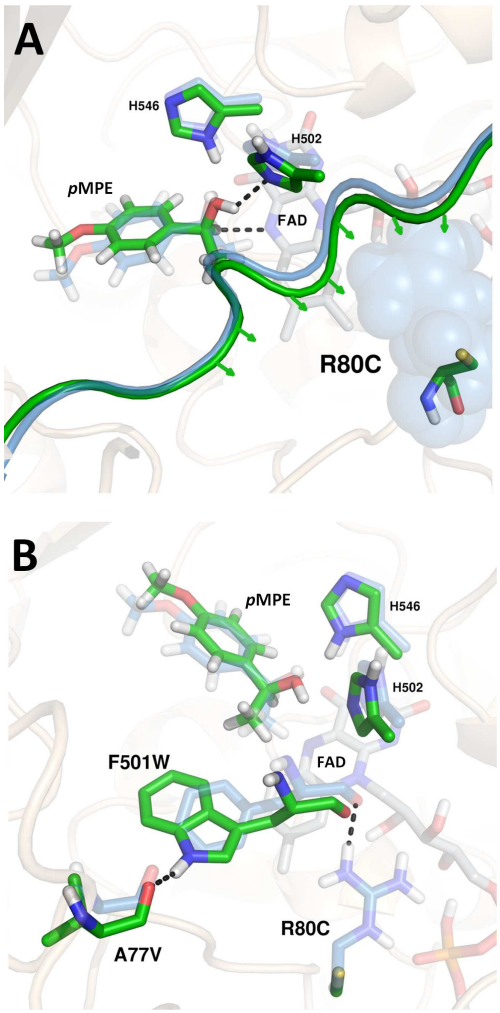

Figure 6. Conformational changes at the catalytic pocket of AAO. (A) Backbone displacement (green) to better position (S)- 1-(p-methoxyphenyl)-ethanol (pMPE). (B) Interruption of the interaction of Arg80 with the backbone of residue 501, and the formation of a hydrogen bond between Val77 and Trp501.

of H_2O_2 in cascade oxyfunctionalization reactions by peroxygenases.[25]

Experimental Section

Materials

All chemicals were reagent-grade purity. Benzyl alcohol, *p*-chlorobenzyl alcohol, 3,4-dimethoxybenzyl alcohol, *p*-Methoxybenzyl alcohol, 1-phenylethanol, 1-phenylpropanol, 1-(*p*-methoxyphenyl)-ethanol, 4-fluoro-α-methylbenzyl alcohol, (R)-4-fluoro-α-methylbenzyl alcohol, (S)-4-fluoro-α-methylbenzyl alcohol, 2,4-hexadien-1-ol, cinnamyl alcohol, Horseradish peroxidase (HRP), Taq polymerase and the Yeast Transformation Kit were purchased from Sigma (Madrid, Spain). Amplex® Red reagent (10-acetyl-3,7-dihydroxyphenoxazine) was obtained from Biogen (Madrid, Spain). Zymoprep Yeast Plasmid Miniprep, Yeast Plasmid Miniprep Kit I and Zymoclean Gel DNA Recovery Kit were from Zymo Research (Orange, CA, USA). Restriction enzymes BamHI and XhoI were from New England Biolabs (Hertfordshire, UK). I-Proof high-fidelity DNA polymerase was from Biorad (Hercules, CA, USA). The episomal shuttle vector pJRoC30 was from the California Institute of Technology (CALTECH, USA). The protease deficient *S. cerevisiae* strain BJ5465 was from LGC Promochem (Barcelona, Spain). E. coli XL2-Blue competent cells were from Stratagene (La Jolla, CA, USA). Primers were acquired from Isogen Life Science (Barcelona, Spain) and are included in Table S1.

Culture Media

Minimal medium SC contained 100 mL 6.7% (w:v) sterile yeast nitrogen base, 100 mL 19.2 g/L sterile yeast synthetic drop-out medium supplement without uracil, 100 mL sterile 20% raffinose (w:v), 700 mL sddH_2O and 1 mL 25 g/L chloramphenicol. YP medium contained 10 g yeast extract, 20 g peptone and ddH_2O to 650 mL whereas YPD medium also contained 20% glucose (w:v). AAO expression medium contained 144 mL YP 1.55×, 13.4 mL 1 M KH_2PO_4 pH 6.0 buffer, 22.2 mL 20% galactose (w:v), 0.222 mL 25 g/L chloramphenicol and ddH_2O to 200 mL. Luria Broth (LB) medium contained 10 g sodium chloride, 5 g yeast extract, 10 g peptone, 1 mL 100 mg/mL ampicillin and ddH_2O to 1 L. AAO selective expression medium (SEM) contained 100 mL 6.7% (w:v) sterile yeast nitrogen base, 100 mL 19.2 g/L sterile yeast synthetic drop-out medium supplement without uracil, 100 mL sterile 20% galactose (w:v), 100 mL 1 M KH_2PO_4 pH 6.0, 600 mL sddH_2O and 1 mL 25 g/L chloramphenicol.

Construction of Variants I500A, F501A and I500A-F501A

All the PCR products were cleaned, concentrated, loaded onto a preparative agarose gel (1%, w:v) and purified using the Zymoclean Gel DNA Recovery kit before being cloned into the shuttle vector pJRoC30 under the control of the GAL1 promoter. BamHI and XhoI were used to linearize the plasmid pJRoC30 and to remove the parent gene. FX9 variant was amplified from pJRoC30-FX9[12b] with two PCR reactions for each mutant containing overhang segments for the whole plasmid to be reassembled in the yeast. PCR reactions were carried out in a final volume of 50 µL containing 3% DMSO, 0.8 mM dNTPs (0.2 mM each), 0.03 U/µL Iproof DNA polymerase, and 0.2 ng/µL template. The oligos used for each PCR reaction were: For I500 A, PCR1 (oligo sense RMLN and oligo antisense I500Ar), PCR2 (oligo sense I500Af and oligo antisense RMLC). For F501 A, PCR1 (RMLN and oligo antisense F501Ar), PCR2 (oligo sense F501Af and RMLC). For double mutant I500A-F501 A, PCR1 (RMLN and oligo antisense DM500-1Ar), PCR2 (oligo sense DM500-1Af and RMLC). Amplification reactions were carried out in a thermal cycler MycyclerTM (BIO-RAD, USA) with the following PCR program: 98 °C for 30 seconds (1 cycle); 98 °C for 10 seconds, 50 °C for 25 seconds and 72 °C for 60 seconds (28 cycles); and 72 °C for ten minutes (1 cycle). After purification, PCR products (400 ng each) were mixed with the linearized pJRoC30 (100 ng; ratio PCR product: vector = 4:1) and transformed in

yeast (Yeast transformation kit) for the recombination and in vivo cloning. 176 colonies were picked, expressed and screened as described below. Each construct was recovered and its sequence confirmed by DNA sequencing.

Directed Evolution

First generation: combinatorial saturation mutagenesis at positions Ile500 and Phe501: Two PCR reactions were carried out in a final volume of 50 µL containing 3% DMSO, 0.8 mM dNTPs (0.2 mM each), 0.03 U/µL iproof DNA polimerase, and 0.2 ng/µL FX9 template and different primers according to the 22-trick protocol.[13] PCR1 contained 0.25 µM RMLN and 0.25 µM mix of reverse primers: 22c1R, 22c2R, 22c3R, 22c4R, 22c5R, 22c6R, 22c7R, 22c8R and 22c9R. PCR2 contained 0.25 µM RMLC and 0.25 µM mix of forward primers: 22c1F, 22c2F, 22c3F, 22c4F, 22c5F, 22c6F, 22c7F, 22c8F and 22c9F. Amplification reactions were carried out in a thermal cycler MycyclerTM (BIO-RAD, USA) with the following PCR program: 98 °C for 30 seconds (1 cycle); 98 °C for 10 seconds, 50 °C for 25 seconds and 72 °C for 60 seconds (28 cycles); and 72 °C for ten minutes (1 cycle). After purification, PCR products (400 ng each) were mixed with the linearized pJRoC30 (100 ng; ratio PCR product: vector = 4:1) and transformed in yeast for in vivo cloning. According to the 22-trick protocol, a library of 3066 individual colonies was screened as described below.

Second generation: MORPHING: The 15G12 variant was used as the parental template for focused random mutagenesis technique MORPHING (Mutagenic Organized Recombination Process by Homologous IN vivo Grouping).[14] Three libraries were constructed independently targeting 3 protein blocks: MA, MB, and MC. Additionally, a mutagenic library subjecting the whole AAO fusion was prepared by error prone PCR (ep-PCR). Primers were designed to create homologous overlapping areas of ~50 bp for the whole gene to be reassembled in vivo upon transformation in S. cerevisiae. i) ep-PCR for MORPHING blocks and whole AAO gene were carried out in a final volume of 50 µL containing: 90 nM oligo sense (FM1 for MA block, FM2 for MB block, FM3 for MC block and RMLN for whole gene amplification), 90 nM oligo antisense (RM1 for fragment MA, RM2 for fragment MB, RM3 for fragment MC and RMLC for whole gene amplification), 0.3 mM dNTPs (0.075 mM each), 3% DMSO, 0.05 or 0.01 mM $MnCl_2$, 1.5 mM $MgCl_2$, 0.05 U/µL Taq polymerase DNA, and 0.92 ng/ µL15G12 template. The amplification parameters were 95 °C for 2 min (1 cycle); 95 °C for 45 s, 50 °C for 45 s, and 74 °C for 2 min (28 cycles); and 74 °C for 10 min (1 cycle). Concentrations of 0.05 and 0.01 mM $MnCl_2$ were used for MORPHING and full gene ep-PCR, respectively, to adjust the mutational rate to 1–3 mutations per gene. ii) High-fidelity PCRs for MORPHING were carried out in a final volume of 50 µL containing 3% DMSO, 0.8 mM dNTPs (0.2 mM each), 0.03 U/µL iproof DNA polimerase, 0.25 µM oligo sense (RMLN for HA1, HB1 and HC fragments, FHF1 for HA2 and FHF2 for HB2), 0.25 µM oligo antisense (RHF1 for HA1, RHF2 for HB1, RHF3 for MC and RMLC for HA2 and HB2 fragments) and 0.2 ng/µL template. High-fidelity PCR was performed using the following parameters: 98 °C for 30 s (1 cycle); 94 °C for 10 s, 48 °C for 30 s, 72 °C for 30 s (30 cycles); and 72 °C for 10 min (1 cycle). The assembly of the fragments for the different libraries is described in Figure 1B. PCR products were cleaned, concentrated, loaded onto a preparative agarose gel, purified, mixed in equimolar amounts, (200 ng mutagenic fragment and 200 ng non-mutagenic fragment) and transformed with linearized pJRoC30 (200 ng) into chemically competent cells, as described above.

Third generation: mutagenic shuffling: ep-PCR reactions were performed separately with mutants 3F10, 11H2, 12D2 and 6G3. Reaction mixtures were prepared in a final volume of 50 µL containing DNA template (0.92 ng/µL), 90 nM oligo sense RMLN (5'-CCTCTATACTTTAACGTCAAGG-3'), 90 nM Reverse primer RMLC (5'-GGGAGGGCGTGAATGTAAGC-3'), 0.3 mM dNTPs (0.075 mM each), 3% (v:v) dimethylsulfoxide (DMSO), 1.5 mM MgCl2, 0.1 mM MnCl2 and 0.05 U/µL Taq DNA polymerase. PCRs were performed in a thermocycler (Mycycler, Bio-Rad, Hercules, CA, USA) and parameters were: 95 °C for 2 min (1 cycle); 95 °C for 45 s, 50 °C for 45 s, 74 °C for 45 s (28 cycles); and 74 °C for 10 min (1 cycle). The PCR products were mixed with linearized pJRoC30 (at a PCR product/linearized plasmid ratio of 4:1) and transformed into competent S. cerevisiae cells to promote in vivo DNA shuffling. Transformed cells were plated on SC (synthetic complete) drop-out plates and incubated for 3 days at 30 °C. Colonies containing the whole autonomously replicating vector were picked and subjected to high-throughput screening as described below.

Fourth generation: site-directed recombination: The 3C11 variant was used as template and primers were designed for the 10 selected mutations (E39G, I76V, A77V, R80C, M83I, V90A, Q174R, F332L, V340A, and Q466R) for the *in vivo* site-directed recombination of mutations vs. corresponding reversions at each position of the combinatorial library. A total of 6 PCR reactions were performed. Reactions were carried out in a final volume of 50 µL containing 3% DMSO, 0.8 mM dNTPs (0.2 mM each), 0.03 U/µL iproof DNA polimerase, and 0.2 ng/ µL 3 C11 with 0.25 µM of the following oligos: PCR1 used oligo sense RMLN and oligo antisense R116 (containing position 39). PCR2 was performed with oligo sense F116 (containing position 39) and oligo antisense R5 (containing positions 76, 77, 80, 83 and 90). PCR3 used oligo sense F5 (containing positions 76, 77, 80, 83 and 90) and oligo antisense R521 (containing position 174). PCR4 used oligo sense F521 (containing position 174) and oligo antisense R9419 (containing positions 332 and 340). PCR5 was performed with oligo sense F9419 (containing positions 332 and 340) and oligo antisense R1397 (containing position 466). PCR6 was performed with oligo sense F1397 (containing position 466) and oligo antisense RMLC, (Figure S1, Table S1). For the in vivo assembly of the whole gene, the fragments were designed with overhangs of around 40 bp between them. Amplification reactions were carried out in a thermal cycler and the PCR program was: 98 °C for 30 seconds (1 cycle); 98 °C for 10 seconds, 50 °C for 25 seconds and 72 °C for 30 seconds (28 cycles); and 72 °C for ten minutes (1 cycle). After purification, PCR products (400 ng each) were mixed with the linearized pJRoC30 (100 ng; ratio PCR product: vector = 4:1) and transformed in yeast for in vivo cloning. A library of 3070 individual colonies was screened as described below.

High-throughput Screening (HTS) Assay

Transformed cells were plated in SC drop-out plates and incubated for 3 days at 30 °C, individual clones were fermented in sterile 96-well plates containing 200 µL of SEM medium. Plates were sealed and incubated at 30 °C, 225 rpm and 80% relative humidity in a humidity shaker (Minitron-INFORS, Biogen, Spain) for 72 hours. Aliquots of 20 µL of yeast supernatants were transferred to a 96-well plate using a robotic station for liquid handling Freedom EVO (Tecan, Männedorf, Switzerland) and 180 µL of HRP-Amplex Red reagent for secondary alcohol activity detection. The final concentrations in the well were 5 mM 1-(*p*-methoxyphenyl)-ethanol, 70 µM Amplex Red, 3 µg/mL HRP in 100 mM phosphate buffer pH 6.0. Reagents were dispensed with Multidrop™ Combi Reagent Dispenser (Thermo Scientific, Massachusetts, USA). The plates were incubated at room temperature and activity with the chiral alcohol was determined as H_2O_2 production coupled to the oxidation of Amplex Red reagent by the HRP and measured at 563 nm ($\varepsilon_{resorufin\ 563} = 56000\ M^{-1}\,cm^{-1}$). Reaction mixture with *p*-methoxybenzyl alcohol (1 mM final concentration) was also prepared to determine activity with a primary alcohol. One unit of AAO activity is defined as the amount of enzyme that converts 1 µmol of alcohol to aldehyde or ketone with the stoichiometric formation of H_2O_2 per min under the reaction conditions. The HTS-assay incorporated two consecutive re-screenings to rule out the selection of false positives as described in previous work.[12a]

Protein Production and Purification

The native AAO, heterologously expressed in *E. coli* and in vitro refolded (wtAAO), was produced and purified as described elsewhere.[15] Evolved variants were produced in yeast[12a] and purified by cationic exchange chromatography, anion exchange chromatography and size-exclusion chromatography (ÄKTA purifier, GE Healthcare, WI, US). The crude extract from *S. cerevisiae* cultures was concentrated and dialyzed in 20 mM sodium phosphate/citrate at pH 3.3 (buffer A) by tangential ultrafiltration (Pellicon; Millipore, USA) through a 10-kDa-pore-size membrane (Millipore, USA) by means of a peristaltic pump (Masterflex easy load; Cole-Parmer, USA). The sample was filtered and loaded onto a strong cation-exchange column (HiTrap SP FF; GE Healthcare) pre-equilibrated with buffer A and coupled to the ÄKTA purifier system. The proteins were eluted with a linear gradient of buffer P (20 mM piperazine buffer pH 5.5) + 1 M NaCl in two phases at a flow rate of 1 ml/min: from 0 to 50% during 15 min and from 50 to 100% in 2 min. Fractions with AAO activity were pooled, dialyzed against buffer P, concentrated and loaded onto a high-resolution resin, strong-anion-exchange column (Biosuite MonoQ 10 cm; Waters, USA) pre-equilibrated in buffer P. The proteins were eluted with a linear gradient from 0 to 0.5 M of NaCl in two phases at a flow rate of 1 ml/min: from 0 to 50% during 20 min and from 50 to 100% in 2 min. Fractions with AAO activity were pooled, dialyzed against 20 mM phosphate buffer pH 6.0, concentrated and further purified by a Superose 12 HR 10/30 molecular exclusion column (Amersham Bioscience; Amersham, UK) pre-equilibrated with 150 mM NaCl in 20 mM phosphate buffer pH 6.0 at a flow rate of 0.5 ml/min. The fractions with AAO activity were pooled, dialyzed against buffer 20 mM phosphate buffer pH 6.0, concentrated and stored.

Biochemical Characterization

Steady-state kinetic constants: Alcohol oxidation kinetics for 1-(*p*-methoxyphenyl)-ethanol, *p*-methoxybenzyl alcohol and 2,4-hexadien-1-ol were measured in 100 mM phosphate buffer pH 6.0 at 25 °C in air-saturated conditions (0.256 mM O_2 concentration). Reactions were performed by triplicate and substrates oxidations were followed by measuring the absorption at 285 nm for *p*-methoxybenzyl alcohol, $\varepsilon_{285} = 16{,}950\ M^{-1}\,cm^{-1}$ and at 280 nm for 2,4-hexadien-1-ol, $\varepsilon_{280} = 30{,}140\ M^{-1}\,cm^{-1}$. The oxidation of 1-(*p*-methoxyphenyl)-ethanol was measured indirectly coupled with saturated conditions of HRP and Amplex Red substrate (4.5 U/mL HRP and 75 µg/mL Amplex Red final concentrations) following activity at 563 nm ($\varepsilon_{563} = 56000\ M^{-1}\,cm^{-1}$).

HPLC analysis and optical rotation: The enantioselectivity of LanDo variant was analyzed by chiral HPLC with equipment consisting of a tertiary pump (Varian/AgilentTechnologies) coupled to an autosampler (Merck Millipore) and a Lux 5 µm Cellulose-1 column (Phenomenex). For the mobile phase hexane and isopropanol in a ratio 9:1 was used. The separation of the enantiomers was performed at a flow rate of 1.0 mL/min. The rotary polarization was measured with a JASCO P-2000 polarimeter. After full conversion, a reaction mixture with the remaining alcohol (1 mg/mL of 1-(p-methoxyphenyl)-ethanol) was extracted with ethyl acetate and dissolved in methanol. The measurement was made at 25 °C with a sodium lamp at 589 nm.

Protein modeling: A structural model of the AAO from *P. eryngii* crystal structure at a resolution of 2.55 Å (Protein Data Bank Europe [PDB] accession number 3FIM,[16] was used as scaffold for the wild type AAO model and the homology models for different mutants were made from 3FIM by PyMol (Schrodinger LLC.; http://www.pymol.org).

DNA sequencing: All genes were verified by DNA sequencing (BigDye Terminator v3.1 Cycle Sequencing Kit) using the following primers: primers sense, RMLN and AAOsec1F and primers antisense RMLC, AAOsec2R, and AAOsec3R.

Computational Methods

The diffusion and binding of the secondary alcohol (S)-1-(*p*-methoxyphenyl)-ethanol were studied using the new adaptive-PELE (Protein Energy Landscape Exploration) software.[17] This adaptive protocol offers improved sampling by running multiple and consecutive short PELE simulations (epochs), setting the initial conditions of each epoch following a reward function that favours sampling of unexplored areas. Even though the ligands were parameterized based on the OPLS2005 force field, the electrostatic charges were derived from the electrostatic potential obtained through quantum calculations at the M06/6-31G* level with Jaguar,[18] and its rotamer library was built with Macromodel.[19] Similarly, the FAD cofactor was optimized with a mixed QM/MM calculation at the same level of theory using Qsite.

A single adaptive-PELE simulation was enough to explore the diffusion and binding of (S)-1-(*p*-methoxyphenyl)-ethanol for the native protein and the different variants. The ligand was initially placed between residues Gly52 and Asn56 in all cases. Each simulation used 192 processors, producing 60 epochs of 20 PELE steps each. During the simulation, ligand perturbations (rotations and translations) are coupled with the backbone perturbation to allow protein flexibility. This is achieved by using an anisotropic network model[20] applied to every Cα atom, while all sidechain conformations within 6 Å of the ligand were predicted each step. An epsilon value of 0.2 was used in the adaptive protocol, meaning that 20% of the processors started each epoch from the structure with the best ligand-FAD distance.

Acknowledgements

This research was supported by the EU project FP7-KBBE-2013-7-613549-INDOX, by the Spanish Government projects BIO2016-79106-R-Lignolution, CTQ2016-74959-R (MINECO/FEDER, EU) and by the Comunidad de Madrid project Y2018/BIO4738-EVOCHIMERA.

References

[1] https://www.statista.com/statistics/263102/pharmaceutical-market-worldwide-revenue-since-2001

[2] a) J. Caldwell, *Hum. Psychopharmacol.* **2001**, *16*, S67-S71; b) B. S. Sekhon, *J. Mod. Med. Chem.* **2013**, *1*, 10–36; c) N. Chhabra, M. L. Aseri, D. Padmanabhan, *Int J App Basic Med Res.* **2013**, *3*, 16–18.

[3] N. M. Maier, P. Franco, W. Lindner, *J. Chromatogr. A* **2001**, *12*, 906(1-2):3-33.

[4] a) K. Faber, *Chemistry.* **2001**, *3*, 7(23):5004-10; b) O. Pàmies, J. E. Bäckvall, *Trends Biotechnol.* **2004**, *22*, 130–5; c) N. J. Turner, *Curr. Opin. Chem. Biol.* **2004**, *8*, 114–9.

[5] a) G. Fantin, M. Fogagnolo, A. Medici, P. Pedrini, S. Poli, M. Sinigaglia, *Tetrahedron Lett.* **1993**, *34*, 883–884; b) Y. L. Li, J. H. Xu, Y. Xu, *J. Mol. Catal. B* **2010**, *64*, 48–52; c) C. Voss, C. Gruber W. Kroutil, *Angew. Chem. Int. Ed.* **2008**, *47*, 741–745.

[6] T. Matsuda, R. Yamanaka, K. Nakamura, *Tetrahedron: Asymmetry.* **2009**, *20*, 513–557.

[7] a) A. Ghanem, H. Y. Aboul-Enein, *Chirality.* **2005**, *17*, 1–15; b) S. Qin, Y. Zhao, B. Wu, B. He, *Appl. Biochem. Biotechnol.* **2016**, *180*, 1456–1466.

[8] a) F. Escalettes, N. J. Turner, *ChemBioChem* **2008**, *14*, 9, 857–60; b) M. M. Musa, K. I. Ziegelmann-Fjeld, C. Vieile, J. G. Zeikus, R. S. Phillips, *J. Org. Chem.* **2007**, *72*, 30–34.

[9] a) W. Kroutil, H. Mang, K. Edegger K. Faber, *Adv. Synth. Catal.* **2004**, *346*, 125–142; b) E. W. van Hellemond, L. Vermote, W. Koolen, T. Sonke, E. Zandvoort, D. P. Heuts, D. B. Janssen, M. W. Fraaije, *Adv. Synth. Catal.* **2009**, *351*, 1523–1530; c) W. P. Dijkman, C. Binda, M. W. Fraaije, A. Mattevi, *ACS Catal.* **2015**, *5*, 1833–1839.

[10] F. J. Ruiz-Dueñas, A. T. Martinez, *Microb. Biotechnol.* **2009**, *2*, 164–77.

[11] P. Ferreira, A. Hernandez-Ortega, B. Herguendas, A. T. Martinez, M. Medina, *J. Biol. Chem.* **2009**, *284*, 24840–24847.

[12] a) J. Viña-Gonzalez, D. Gonzalez-Perez, P. Ferreira, A. T. Martinez, M. Alcalde, *Appl. Environ. Microbiol.* **2015**, *81*, 6451–62; b) J. Viña-Gonzalez, K. Elbl, X. Ponte, F. Valero, M. Alcalde, *Biotechnol. Bioeng.* **2018**, *115*, 1666–1674.

[13] S. Kille, C. G. Acevedo-Rocha, L. P. Parra, Z. G. Zhang, D. J. Opperman, M. T. Reetz, J. P. Acevedo, *ACS Synth. Biol.* **2013**, *2*, 83–92.

[14] D. Gonzalez-Perez, P. Molina-Espeja, E. Garcia-Ruiz, M. Alcalde, *PLoS One.* **2014**, *9*, e90919.

[15] F. J. Ruiz Dueñas, P. Ferreira, M. J. Martínez, A. T. Martínez, *Prot. Exp. Purif.* **2006**, *45*, 191–199.

[16] I. S. Fernandez, F. J. Ruiz-Dueñas, E. Santillana, P. Ferreira, M. J. Martinez, A. T. Martinez, A. Romero, *Acta Crystallogr. Sect. C* **2009**, *65*, 1196–1205.

[17] D. Lecina, J. F. Gilabert, V. Guallar, *Sci. Rep.* **2017**, *7*, 8466.

[18] A. D. Bochevarov, E. Harder, T. F. Hughes, J. R. Greenwood, D. A. Braden, D. M. Philipp, D. Rinaldo, M. D. Halls, J. Zhang, R. A. Friesner, *Int. J. Quantum Chem.* **2013**, *113*, 2110–2142.

[19] a) R. B. Murphy, D. M. Philipp, R. A. Friesner, *J. Comput. Chem.* **2000**, *21*, 1442–1457; b) G. M. Sastry, M. Adzhigirey, T. Day, R. Annabhimoju, W. Sherman, *J. Comput.-Aided Mol. Des.* **2013**, *27*, 221–234.

[20] A. R. Atilgan, S. R. Durell, R. L. Jernigan, M. C. Demirel, O. Keskin, I. Bahar, *Biophys. J.* **2001**, *80*, 505–515.

[21] A. Hernandez-Ortega, P. Ferreira, A. T. Martinez, *Appl. Microbiol. Biotechnol.* **2012**, *93*, 1395–1410.

[22] A. Serrano, F. Sancho, a J. Viña-González, J. Carro, M. Alcalde, V. Guallar, A. T. Martínez, *Catal. Sci. Technol.* **2019**, *9*, 833–841.

[23] A. Hernandez-Ortega, P. Ferreira, P. Merino, M. Medina, V. Guallar, A. T. Acta Crystallogr. Sect. DMartinez, *ChemBioChem.* **2012**, *13*, 427–435.

[24] a) P. Ferreira, F. J. Ruiz-Dueñas, M. J. Martinez, W. J. H. van Berkel, A. T. Martínez, *FEBS J.* **2006**, *273*, 4878–4888; b) A. Hernandez-Ortega, F. Lucas, P. Ferreira, M. Medina, V. Guallar, A. T. Martinez, *Biochemistry.* **2012**, *51*, 6595–6608; c) J. Carro, P. Amengual-Rigo, F. Sancho, M. Medina, V. Guallar, P. Ferreira, A. T. Martínez, *Sci. Rep.* **2018**, *8*, 8121.

[25] J. Carro, E. Fernandez-Fueyo, C. Fernandez-Alonso, J. Cañada, R. Ullrich, M. Hofrichter, M. Alcalde, P. Ferreira, A. T. Martinez, *Biotechnol. Biofuels* **2018**, *11*, 86.

[26] P. Ferreira, M. Medina, F. Guillén, M.J. Martínez, W. J. Van Berkel, A. T. Martínez, *Biochem. J.* **2005**, *1*, 731–8.

Advanced Synthesis & Catalysis

Supporting Information

Structure-Guided Evolution of Aryl Alcohol Oxidase from *Pleurotus eryngii* for the Selective Oxidation of Secondary Benzyl Alcohols

Javier Viña-Gonzalez, Diego Jimenez-Lalana, Ferran Sancho, Ana Serrano, Angel T. Martinez, Victor Guallar, and Miguel Alcalde*

Supporting information for:

Structure-Guided Evolution of Aryl Alcohol Oxidase from *Pleurotus eryngii* for the Selective Oxidation of Secondary Benzyl Alcohols

Javier Viña-Gonzalez[1], Diego Jimenez-Lalana[1], Ferran Sancho[2], Ana Serrano[3], Angel T. Martinez[3], Victor Guallar[2,4] and Miguel Alcalde[1*]

[1]Department of Biocatalysis, Institute of Catalysis, CSIC, Cantoblanco, 28049 Madrid, Spain.

[2]Barcelona Supercomputing Center, Jordi Girona 31, 08034 Barcelona, Spain.

[3]Biological Research Center, CSIC, Ramiro de Maeztu 9, 28040 Madrid, Spain.

[4]ICREA, Passeig Lluís Companys 23, 08010 Barcelona, Spain.

*Corresponding author: malcalde@icp.csic.es

Table of contents

Supporting Table 1. List of primers

Oligo	Sequence
RMLN	5’-CCTCTATACTTTAACGTCAAGG-3’
RMLC	5’-GGGAGGGCGTGAATGTAAGC-3’
I500Af	5’- GAGACAACGCCAACACG*GCT*TTCCACCCAGTTGGAACGGC -3’
I500Ar	5’- GCCGTTCCAACTGGGTG*GAA*AGCCGTGTTGGCGTTGTCTC -3’
F501Af	5’-GAGACAACGCCAACACGATT*GCT*CACCCAGTTGGAACGGC -3’
F501Ar	5’- GCCGTTCCAACTGGGTGAGC*AAT*CGTGTTGGCGTTGTCTC -3’
DM5001Af	5’- GAGACAACGCCAACACG*GCTGCT*CACCCAGTTGGAACGGC -3’
DM5001Ar	5’- GCCGTTCCAACTGGGTG*AGCAGC*CGTGTTGGCGTTGTCTC -3’
22c1F	5’-GAGACAACGCCAACACG*NDTNDT*CACCCAGTTGGAAC-3’
22c1R	5’-GTTCCAACTGGGTG*AHNAHN*CGTGTTGGCGTTGTCTC-3’
22c2F	5’-GAGACAACGCCAACACG*NDTVHG*CACCCAGTTGGAAC-3’
22c2R	5’-GTTCCAACTGGGTG*CDBAHN*CGTGTTGGCGTTGTCTC-3’
22c3F	5’-GAGACAACGCCAACACG*NDTTGG*CACCCAGTTGGAAC-3’
22c3R	5’-GTTCCAACTGGGTG*CCAAHN*CGTGTTGGCGTTGTCTC-3’
22c4F	5’-GAGACAACGCCAACACG*VHGNDT*CACCCAGTTGGAAC-3’
22c4R	5’-GTTCCAACTGGGTG*AHNCDB*CGTGTTGGCGTTGTCTC-3’
22c5F	5’-GAGACAACGCCAACACG*VHGVHG*CACCCAGTTGGAAC-3’
22c5R	5’-GTTCCAACTGGGTG*CDBCDBC*GTGTTGGCGTTGTCTC-3’
22c6F	5’-GAGACAACGCCAACACG*VHGTGG*CACCCAGTTGGAAC-3’
22c6R	5’-GTTCCAACTGGGTG*CCACDB*CGTGTTGGCGTTGTCTC-3’
22c7F	5’-GAGACAACGCCAACACG*TGGNDT*CACCCAGTTGGAAC-3’
22c7R	5’-GTTCCAACTGGGTG*AHNCCA*CGTGTTGGCGTTGTCTC-3’
22c8F	5’-GAGACAACGCCAACACG*TGGVHG*CACCCAGTTGGAAC-3’
22c8R	5’-GTTCCAACTGGGTG*CDBCCA*CGTGTTGGCGTTGTCTC-3’

22c9F	5’-GAGACAACGCCAACACG*TGGTGG*CACCCAGTTGGAAC-3’
22c9R	5’-GTTCCAACTGGGTG*CCACCA*CGTGTTGGCGTTGTCTC-3’
RHF1	5’-GGAACAAGGCCGGGCGCAAG-3’
FM1	5’-TAGGGGCAGAGGCTCCACTC-3’
RM1	5’-GCATAGCGATCGAAATCTTC-3’
FHF-1	5’-TCATGATGCGTGGATCAACA-3’
RHF-2	5’-AGGAGCAAATGGTCGGATAG-3’
FM2	5’-ATCCTAGCGTAGGCCGAAAC-3’
RM2	5’-TCTCCGCGAGCTACAGGAGA-3’
FHF-2	5’-TTATGAGTGTTACAAACGCGTTGATT-3’
RHF-3	5’-GTTGGCGTTGTCTCTAATGTACGACTC-3’
FM3	5’-CGACGGACGATGCTGCTATC-3’
F116	5’-ACGTGTCCGTCTTGGTCCTAGAGGCGGGTGTATCAGAT*GRG*AA-‘3
R116	5’-TCTGCCCCTAATACATT*CYC*A-‘3
F5	5’-CA*RTTGYG*TATCCT*YGC*GGCCGT*ATR*CTAGGGGGGTCTAGCTCT*GYT*AA-‘3
R5	5’-TT*ARC*AGAGCTAGACCCCCCTAG*YAT*ACGGCC*GCR*AGGATA*CRCAAY*TG-‘3
F521	5’- GCGTCATGGCCACGACG*CRA*GAGCAAA-‘3
R521	5`- GTCGGGATTGAAGAAGAACTCTTCGCTTTGCTC*TYG*CGTCGTGG -‘3
F9419	5’-ATAACATC*YTC*AGAGACTCGTCCGAGTTCAAC*GYT*GATTTA-‘3
R9419	5’-TAAATC*ARC*GTTGAACTCGGACGAGTCTCT*GAR*GATGTTAT-‘3
F1397	5’-TTCGTTTCCTCTCTGGT*CRA*GC-‘3
R1397	5’-GTATAACGAAGTCCGCCCACGC*TYG*ACC-’3
AAOsec1F	5’-GTGGATCAACAGAAGATTTCGATCG-3’
AAOsec2R	5’-GTGGTTAGCAATGAGCGCGG-3’
AAOsec3R	5’-GGAGTCGAGCCTCTGCCCCT-3’

Codon substitutions are shown in italics (where N = A/T/C/G; D = no C; V =no T, H = no G; B = no A; R = A/G; Y = C,T).

Supporting Table 2. Polarimeter measurements for the LanDo variant reaction with 1-(*p*-methoxyphenyl)-ethanol (correspondent to the remaining R-enantiomer). Number of cycles: 8 with 1 sec cycle iterval. Path length 100mm.

PMT Voltage[V]	Temperature[ºC]	Optical Rotation Monitor
353	24.96	0.0592
353	24.95	0.0601
353	24.96	0.0593
354	24.96	0.0602
353	24.98	0.0586
353	24.99	0.0603
354	25.01	0.0600
354	25.03	0.0589

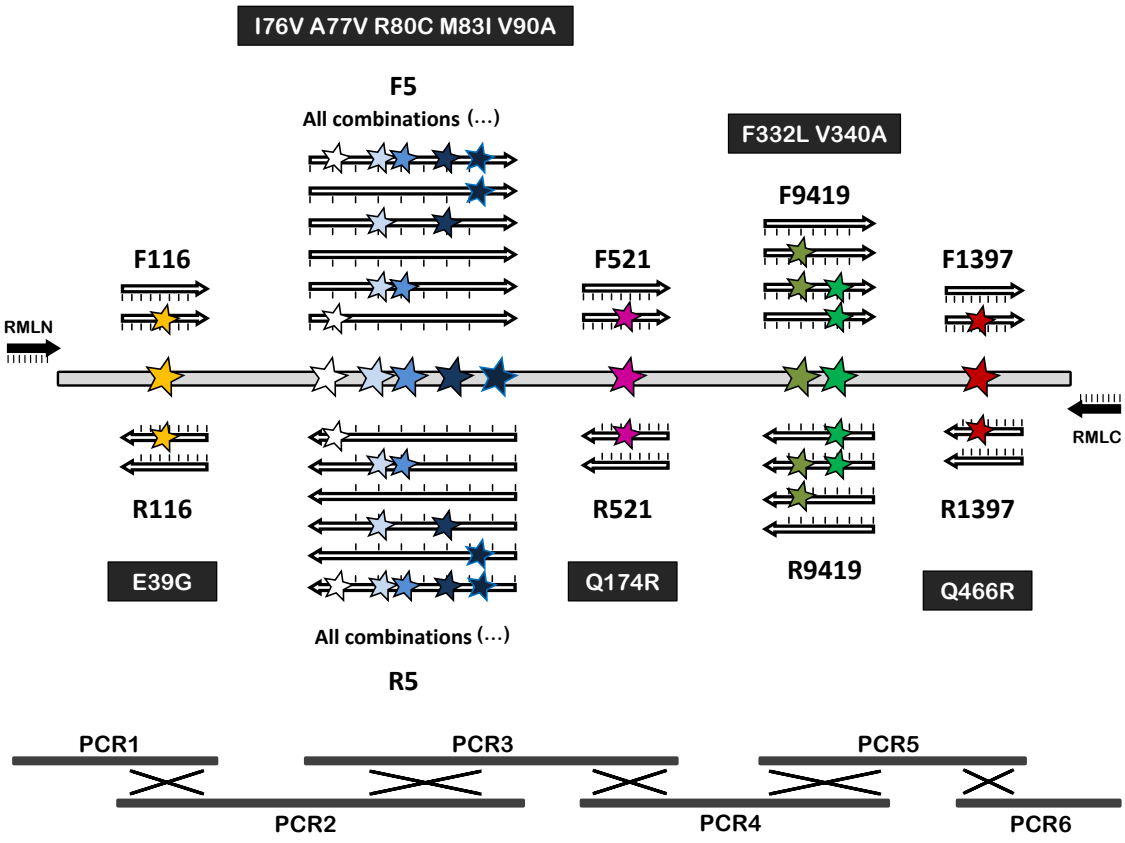

Figure S1. Method for *in vivo* site-directed recombination. Primers designed to be used in the site-directed recombination experiment for the PCR amplification of the selected mutated positions (in black). For each mutation, adjacent sense and antisense primers were synthesized that were 50% mutated at the sites of interest. Six PCR reactions were performed with ~40 bp homologous sequences at each end to foster *in vivo* recombination (7 crossover events). The PCR fragments were assembled by transformation into yeast with the linearized vector to yield a library of all combinations of the mutations/reversions in one-pot .

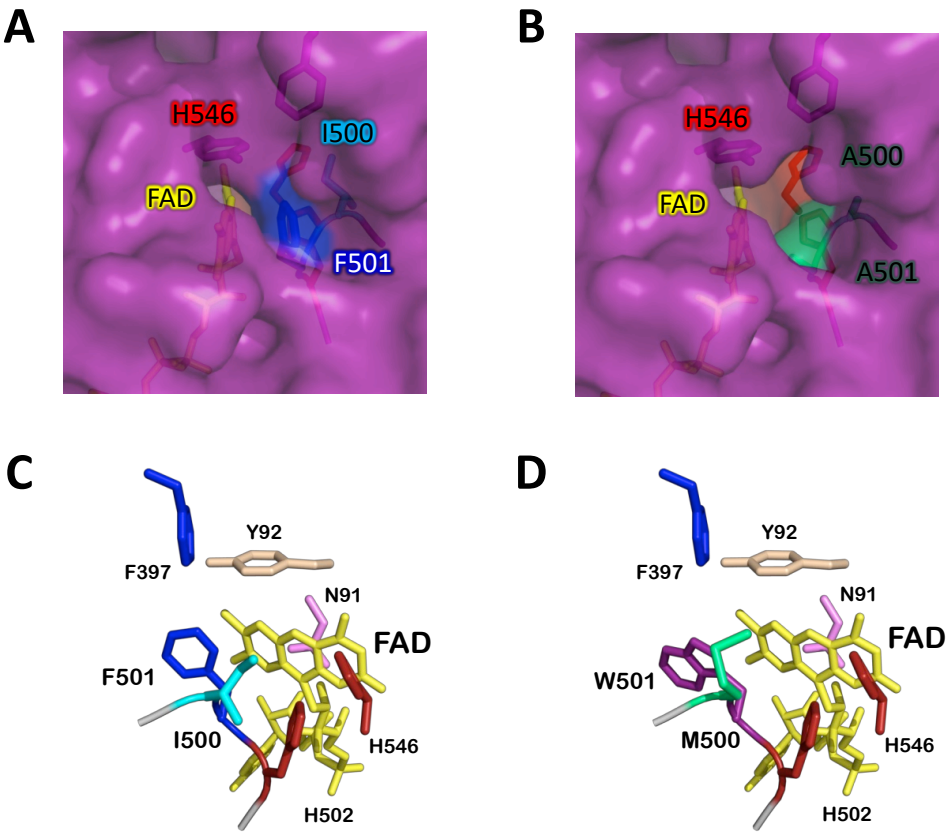

Figure S2. The access channel and catalytic pocket before and after mutation. The channel giving access to the active site in the FX9 (**A**) and I500A-F501A (**B**) mutants: the FAD molecule is depicted in yellow, the Phe501 and Ile500 residues in the parental type are in blue and light blue, the Ala500 and Ala501 mutations are in green, and histidine 546 at the catalytic pocket is in red. Catalytic pocket in the FX9 (**C**) and 15G12 (**D**) variants: His502 and His546 at the active site are depicted in red, FAD is depicted in yellow, ancestral/consensus mutation Asn91 is in pink, Phe397 and Phe501 are in blue, Ile500 in light blue, Tyr92 is depicted in white, whereas the new Trp501 and Met500 substitutions are depicted in purple and light green, respectively. The models were prepared from the crystal structure of *P. eryngii* AAO (PDB 3FIM).

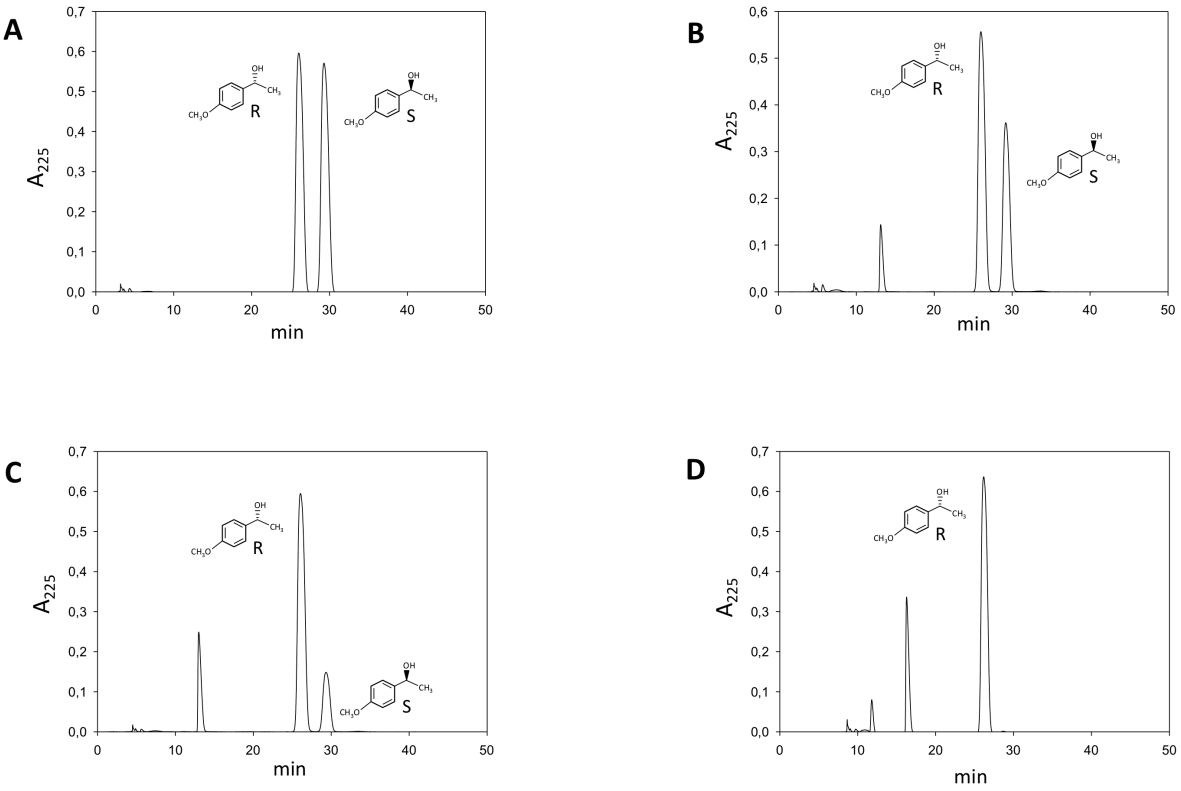

Figure S3. **Chiral HPLC chromatograms**. Elution profiles of the reaction of LanDo variant (1 µM) with racemic 1-(*p*-methoxyphenyl)-ethanol (2.5 mM). Negative control (A), after 15 minutes reaction (B), after 45 min reaction (C) and after 90 min reaction (D).